Critical temperatures for radiation enhanced diffusion and metastable alloy formation in ion beam mixing

R. de Reus *, A.M. Vredenberg, A.C. Voorrips, H.C. Tissink, and F.W. Saris

FOM-Institute for Atomic and Molecular Physics, Kruislaan 407, 1098 SJ Amsterdam, The Netherlands

Phase formation, stability, and mixing behavior in the metallic systems Ni–Zr, Fe–Zr, Au–Zr, and Pd–Ta have been investigated under influence of high energy heavy ion beams as a function of temperature. Our results and data from the literature support a simple model which correlates onset temperatures for radiation enhanced diffusion and equilibrium phase formation in ion beam mixing with hole (or vacancy) formation enthalpies. The model offers the possibility to predict temperature ranges in which efficient mixing occurs by radiation enhanced diffusion without formation of stable alloys.

1. Introduction

As first shown by Matteson et al. [1], two different temperature regimes can be distinguished in ion beam mixing. At low temperatures ion beam mixing appears to be temperature independent. In this regime the majority of atomic mixing takes place in well developed collision cascades on time scales of 10^{-11} s. The quantity of intermixed material depends, among others, on the chemical affinity of the elements being mixed [2–6]. A large negative heat of mixing will facilitate the mixing process, whereas a large positive heat of formation will hinder ion mixing. At low temperatures no long range diffusion is possible and metastable phases are formed in almost every case [6,7]. With the aid of Miedema's macroscopic atom model [8] one can compare the thermodynamics of amorphous phases and solid solutions. As shown by Loeff et al. [9], this provides an easy tool in predicting the glass forming range for an arbitrary system consisting of two transition metals. The lower Gibbs free energy determines which metastable phase is expected to form: either the amorphous phase or a (supersaturated) solid solution.

In the higher temperature regime ion mixing becomes strongly temperature dependent. The general belief is that a thermally activated long range diffusion process sets in when defects, generated by the incoming ions, become mobile. This is called radiation enhanced diffusion (RED). The critical temperature for RED, T_c, is defined as the temperature at which the temperature-

dependent mixing equals the temperature-independent cascade mixing process. Recently, correlation between cohesive energy and T_c has been convincingly shown [10,11]. It was demonstrated that T_c (in kelvin) is proportional to the activation energy, Q_{RED}, of the effective diffusion coefficient of radiation enhanced diffusion. On the assumption that Q_{RED} scales with the cohesive energy of solids, E_{coh}, one arrives at the proportionality between T_c and E_{coh}. The cohesive energy is the energy required to disassemble a solid into its constituent atoms. In refs. [10] and [11] the cohesive energy was chosen as the average of the cohesive energies of the elements being mixed.

For elementary metals it has been shown [12] that the heat of formation of monovacancies is proportional to the cohesive energy: $\Delta H_{1v} = -0.29E_{coh}$. In a binary alloy one can distinguish between two types of holes (or vacancies), namely ΔH_{VA} and ΔH_{VB}, corresponding to holes the size of A- and B-atoms respectively. If there is a large difference between ΔH_{VA} and ΔH_{VB} (e.g. in the systems Ni–Zr, Fe–Zr, Au–Zr), two critical temperatures are expected in ion beam mixing, one correlated with ΔH_{VA}, the other with ΔH_{VB}. The lowest critical temperature is correlated with the formation of holes the size of the smaller constituent, ΔH_{Vsmall}. We identify this temperature as T_c, for radiation enhanced diffusion sets in when the smaller constituent of the alloy becomes mobile. Although RED occurs, this does not necessarily drive the system to equilibrium, as has been shown in several studies on RED in amorphous alloys [13–16]. To form crystal structures of equilibrium compounds collective motion of both constituents is required, as first shown by Schwarz and Johnson and later by other authors [17]. Therefore, a second critical

temperature in ion beam mixing should exist which is correlated with the formation enthalpy of holes the size of the larger constituent, ΔH_{Vlarge}. Above this critical temperature, which we call T_{eq}, formation of equilibrium compounds is expected.

In this paper we will show evidence for these two critical temperatures in the systems Ni–Zr, Fe–Zr, and Au–Zr. Values of T_c have been determined by Ding et al. [14–16]. Using transmission electron microscopy (TEM), we have observed that above T_c the alloys were still amorphous, in agreement with the model proposed above. Furthermore, for these systems we have determined, by means of TEM, at which temperature equilibrium phases form.

Only one critical temperature ($T_c = T_{\text{eq}}$) is expected in ion beam mixing of binary alloys for which ΔH_{Vsmall} is approximately the same as ΔH_{Vlarge}. First this is verified in the system Pd–Ta and then the correlations of T_c and T_{eq} with ΔH_{Vsmall} and ΔH_{Vlarge} respectively are compared with available data from literature.

2. Experimental

Thin metal films were deposited in a dual e-gun evaporation system with a base pressure less than 5×10^{-9} mbar. At a typical deposition rate of 3 Å/s the pressure rose to a maximum of 1×10^7 mbar. The substrates, oxidized silicon wafers and cleaved NaCl single crystals, were kept at liquid nitrogen temperature during deposition. Amorphous $Ni_{55}Zr_{45}$, $Fe_{55}Zr_{45}$, $Au_{50}Zr_{50}$, and $Au_{35}Zr_{65}$ films were deposited onto NaCl substrates. The composition of the alloys was chosen such that the highest crystallization temperature is expected [18–22]. Not much is known about amorphous Au–Zr, but according to a model proposed by Barbour et al. [17], a higher stability is expected for amorphous $Au_{35}Zr_{65}$ compared to the $Au_{50}Zr_{50}$ alloy. The total thickness of the films, measured by Rutherford backscattering spectroscopy (RBS), was usually about 500 Å. Impurity concentrations of light elements like oxygen, carbon, and nitrogen, were found to be below the detection limit for RBS.

Pd–Ta was studied using multilayer samples. Alternating layers of elemental Pd (35 Å) and Ta (65 Å) were deposited to a total thickness of 500 Å onto NaCl single crystals. Complete mixing of the multilayered samples would result in an alloy with a composition $Pd_{40}Ta_{60}$, which has been shown to be close to the most stable composition for both thermal annealed and ion irradiated amorphous Pd–Ta at elevated temperatures [23]. To study the temperature dependence of ion beam mixing in the Pd–Ta system, also a bilayer structure of 450 Å Pd/400 Å Ta was deposited onto an oxidized silicon wafer. The Ta layer was evaporated on top to avoid

reaction with the SiO_2 substrate and for better separation of the peaks in RBS analysis.

Before ion irradiation, TEM samples were prepared by floating off the NaCl substrates in deionized water and picking up the metal films on molybdenum TEM grids.

Ion mixing experiments were performed by mounting the samples on a molybdenum block, which could be heated in the temperature range from room temperature to 800°C by radiative heating with a hot filament at the backside. The temperature was measured by a pyrometer at the front side of the block, and a platinum resistance inside the block. The accuracy of the temperature measurement of the samples is estimated to be within ± 50°C. A single ended Van de Graaff accelerator [24] was used to produce an 825 keV $^{129}Xe^+$ ion beam for the ion irradiations. To minimize beam heating effects, the beam current was kept at 70 nA/cm². The total fluence was between 0.4 and 5.0×10^{15} ions/cm². A dose of 1.5×10^{15} ions/cm² results in 10 displacements per Zr atom in the Zr-based alloys, as calculated by the TRIM-86 computer code [25]. During irradiation the vacuum was better than 1×10^{-7} mbar. In all cases a reference sample was also mounted on the block. These samples were subjected to the same heat treatment as the irradiated samples, but were screened from the ion beam. After irradiation the samples were cooled to room temperature and examined by TEM and RBS with 2 MeV He^+. The RBS analysis was done using the RUMP computer code [26].

3. Results

3.1. Ni–Zr, Fe–Zr, and Au–Zr

The Zr-alloys were found to show a very similar behavior. All alloys were amorphous as deposited. This is based on observations with TEM: bright field images are structureless and in diffraction mode broad halos are observed. Also, dark field images are homogeneous and structureless.

In fig. 1 TEM results of the $Ni_{55}Zr_{45}$ amorphous alloy are shown after ion mixing at elevated temperatures with 825 keV $^{129}Xe^+$ ions to a dose of 1.5×10^{15} ions/cm². Fig. 1(a) shows that after ion mixing at room temperature the alloy is amorphous. The fainter weak halo in the diffraction pattern indicates that also an amorphous oxide has formed. The formation of an oxide becomes clearer after ion mixing at 570 K [fig. 1(b)]. The pictures taken at this temperature are representative for all Ni–Zr samples irradiated between 370 and 620 K. At these measurements the Ni–Zr alloy is still amorphous, but also the metastable γ-ZrO_2 phase [27] is observed. Note that no crystalline Ni–Zr phases are observed, even though irradiations are performed at

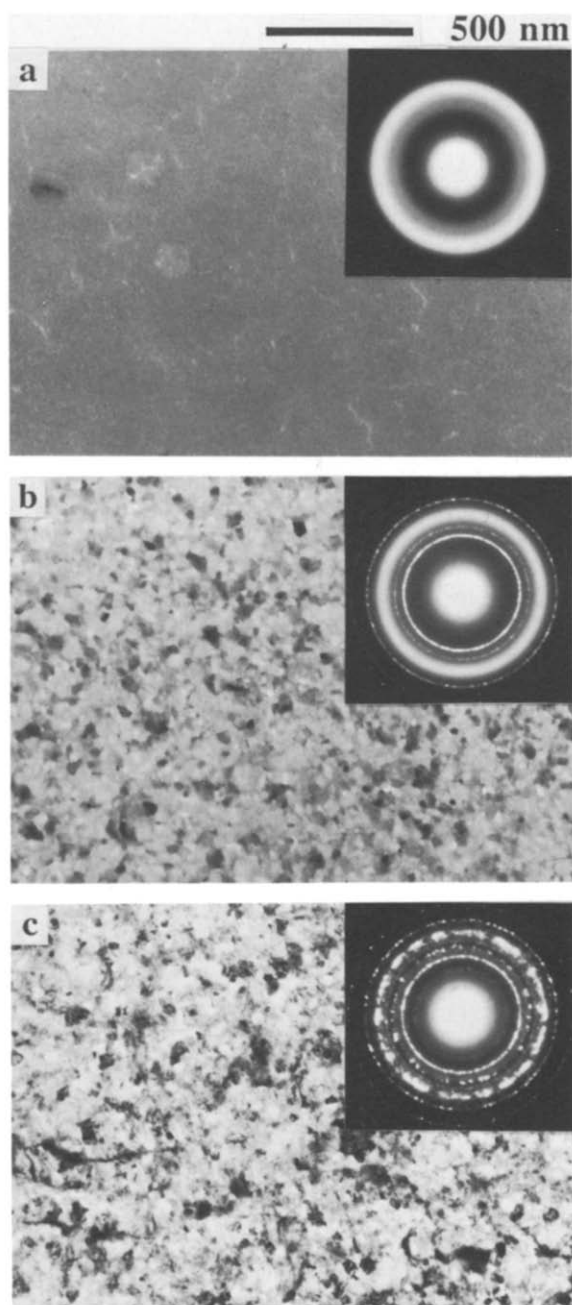Fig. 1. Phase formation in amorphous $Ni_{55}Zr_{45}$ during ion beam mixing with 825 keV Xe^+ ions to a dose of 1.5×10^{15} ions/cm². TEM bright field images and diffraction patterns show that after irradiation: (a) at room temperature the alloy is amorphous; (b) after irradiation between 370 and 620 K amorphous Ni–Zr and γ-ZrO_2 are observed; the measurement is taken of a sample after irradiation at 570 K; (c) after irradiation at temperatures of 650 K or higher the amorphous alloy has crystallized into the equilibrium compounds Ni_2Zr and Ni_5Zr. Also γ-ZrO_2 is observed; the measurement is taken after ion irradiation at 650 K.

temperatures far in the regime of RED, which sets in at $T_c \approx 460$ K [14]. During ion mixing at 650 K [fig. 1(c)] and higher temperatures crystallization into Ni_2Zr and Ni_5Zr intermetallic compounds [28] occurred. In addition the γ-ZrO_2 phase is observed. For T_{eq} we took a value of 650 K. The crystallization temperature of amorphous $Ni_{55}Zr_{45}$ is considerably lowered by ion irradiation. Only at 770 K the reference samples, which were only subjected to thermal treatment, crystallized into the intermetallics Ni_2Zr and $Ni_{10}Zr_7$ [28]. At this temperature also diffraction lines of γ-ZrO_2 are observed. The crystallization data of the thermally treated Ni–Zr alloys agree well with literature data [19,20]. Note that the equilibrium phases formed by thermal annealing are slightly different from those formed during ion irradiation, probably because of small composition changes during oxidation.

Although a rather strong oxidation is observed, we believe that the effects on the crystallization process are small. It has been shown for several amorphous alloys that oxygen contamination strongly enhances the thermal stability [29]. However, oxidation during ion mixing of Fe–Zr at elevated temperatures has also been observed by Bøttiger et al. [30], who showed that the oxidation effects were restricted to the sample surface. Surface oxidation of Ni–Zr alloys has been observed during thermal annealing in oxygen ambient [31,32]. The effect of surface oxidation is the formation of stoichiometric Zr-oxides at the sample surface. As a consequence the underlying alloy slightly changes composition but its thermal stability is not affected.

The TEM micrographs of the amorphous $Fe_{55}Zr_{45}$ alloy in fig. 2 show similarity with the Ni–Zr system. After ion irradiation between room temperature and 670 K [figs. 2(a) and 2(b)] amorphous Fe–Zr and γ-ZrO_2 are identified. Electron microprobe analysis showed that the oxygen content of both the irradiated and annealed samples increased to roughly 10 at%. In reference samples, annealed at the same temperature, no diffraction lines of γ-ZrO_2 are observed with TEM, probably because the oxide formed is amorphous whereas during ion irradiation the crystalline phase γ-ZrO_2 appears. Primary crystallization of the amorphous Fe–Zr phase occurs at approximately 720 K into the tetragonal Fe_2Zr compound [33] during ion irradiation, as can be seen from fig. 2(c). The same crystallization process is observed in the reference samples after annealing at 870 K, in agreement with literature data [21,22]. No crystalline phases are detected below the crystallization temperature during thermal annealing. Like Ni–Zr, also Fe–Zr remains amorphous under influence of the ion beam up to temperatures far above T_c, which is approximately 480 K [15].

As can be seen in fig. 3, the same type of behavior is also observed for the Au–Zr system. Results are shown for the amorphous $Au_{50}Zr_{50}$ alloy after irradiation at

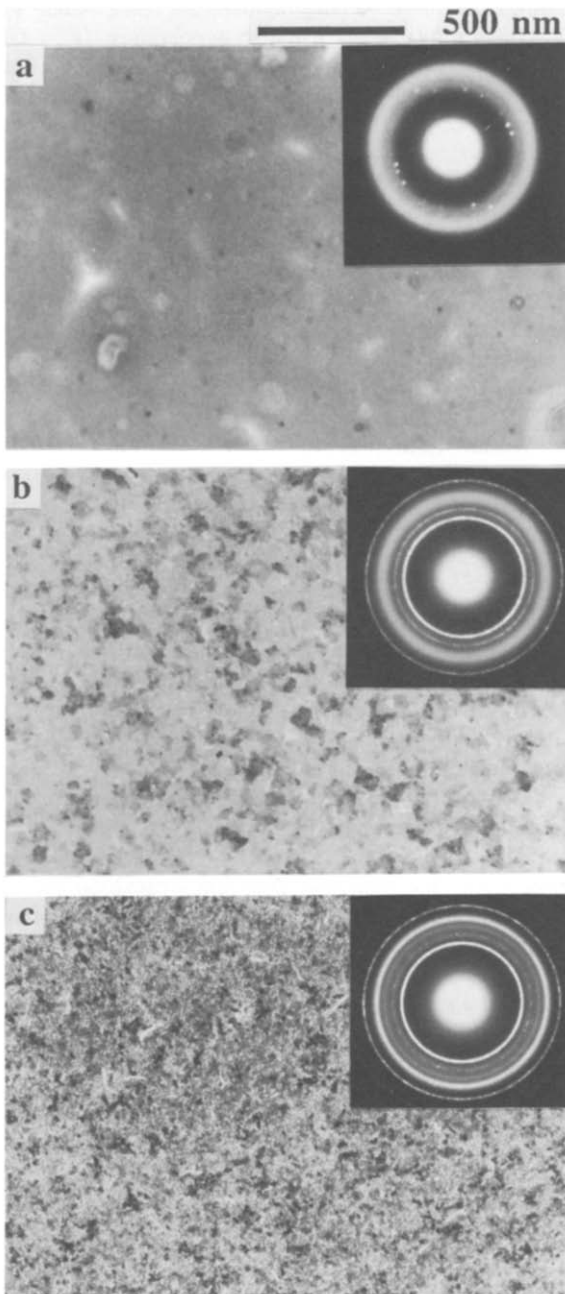Fig. 2. Phase formation in amorphous $Fe_{55}Zr_{45}$ during ion beam mixing with 825 keV Xe^+ ions to a dose of 1.5×10^{15} ions/cm². TEM bright field images and diffraction patterns show that after irradiation: (a) at room temperature amorphous Fe–Zr and some γ-ZrO_2 is observed; (b) after ion mixing up to temperatures of 670 K amorphous Fe–Zr is observed and γ-ZrO_2 has formed; the pictures are from a sample irradiated at 670 K; (c) at temperatures of 720 K and higher hexagonal Fe_2Zr and γ-ZrO_2 have formed; the measurement is from a sample irradiated at 720 K.
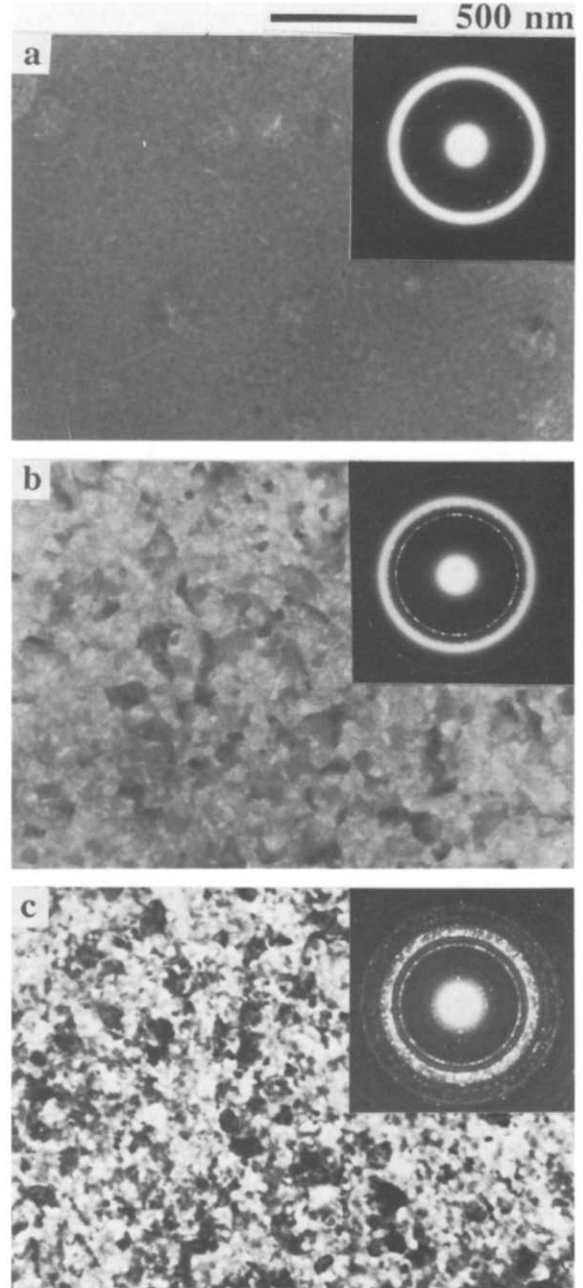
Fig. 3. Phase formation in amorphous $Au_{50}Zr_{50}$ during ion beam mixing with 825 keV Xe^+ ions to a dose of 1.5×10^{15} ions/cm². TEM bright field images and diffraction patterns show that after irradiation: (a) at room temperature the Au–Zr is still amorphous and some γ-ZrO_2 has formed; (b) after irradiations between 370 and 570 K amorphous Au–Zr and γ-ZrO_2 are observed (pictures taken after irradiation at 570 K), whereas (c) after ion irradiation at 620 K and higher the amorphous alloy has crystallized into an unidentified Au–Zr phase; also γ-ZrO_2 is observed.

room temperature, 570 K, and 620 K respectively. Up to 570 K only amorphous Au–Zr and γ-ZrO$_2$ are observed, whereas at temperatures of 620 K and higher crystallization into an unidentified phase occurs. Thermal annealing without ion irradiation leads to crystallization at 720 K into the same unidentified phase. In a second set of samples with a composition of Au$_{35}$Zr$_{65}$, crystallization into the Au$_4$Zr equilibrium phase [34] is observed to occur at 670 K during ion irradiation, and at 770 K during thermal annealing. Also amorphous Au–Zr is found to be stable under ion irradiation far above the critical temperature for RED, which is $T_c \approx$ 450 K [16].

3.2. Pd–Ta

A summary of the results of ion mixing of the Pd-Ta bilayers is presented in fig. 4, where the squares of the normalized diffusion distances, $(\Delta x)^2$, are plotted in Arrhenius fashion. The mixing experiments were performed with 825 keV ^{129}Xe$^+$ ions with fluences varying between 0.4×10^{15} and 5.0×10^{15} ions/cm^2. The thickness Δx of the intermixed layer is inferred from RBS spectra (not shown). Δx is determined as the thickness between heights of 16% and 84% of the gradually changing concentration profile due to intermixing at the interface. The data in fig. 4 are scaled to a dose of 1×10^{15} ions/cm^2. As can be seen from fig. 4, the
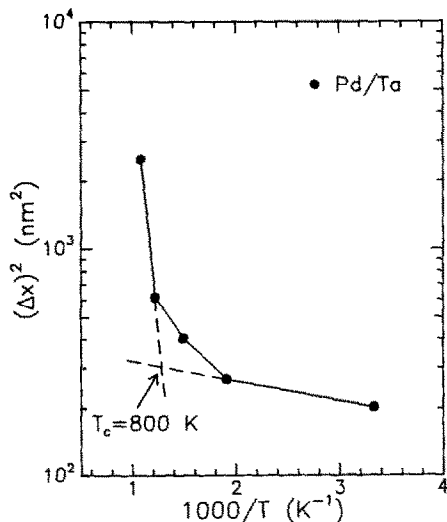

Fig. 4. The temperature dependence of ion beam mixing of a Pd/Ta bilayer with 825 keV Xe$^+$ ions. The thickness Δx of the intermixed layer is scaled to a dose of 1×10^{15} ions/cm^2. At high temperatures the mixing behavior is strongly temperature dependent. The critical temperature for RED, $T_c =$ 800(± 75) K is determined by the intercept of the extrapolated temperature-dependent and temperature-independent parts of the Arrhenius-curve.

mixing behavior is almost temperature independent at low temperatures, whereas at high temperatures ($T > 800$ K) a strong temperature dependence is observed. The critical temperature for RED is taken as the intercept of the extrapolated temperature-dependent and temperature-independent contributions in the Arrhenius-curve of fig. 4. We find for ion beam mixing of Pd/Ta bilayers that $T_c \approx$ 800 K (± 75 K). After ion irradiation up to temperatures of 820 K the intermixed layer shows a gradual change in the concentration profile. After ion irradiation at 920 K and higher temperatures plateaus in the RBS spectra indicate phase formation.

Phase formation is studied in multilayer samples of elemental Pd and Ta with an overall composition of Pd$_{40}$Ta$_{60}$. The phase formation is shown in fig. 5. In the as-deposited films (not shown) only the Pd and α-Ta phases [35,36] with a grain size less than 100 Å are observed. After irradiation between room temperature and 520 K, the film is completely amorphized for fluences higher than approximately 4×10^{15} ions/cm^2 [fig. 5(a)]. At higher temperatures an amorphous alloy and a supersaturated solid solution of Pd(Ta) are formed. Fig. 5(b) shows such a sample after ion mixing at 670 K. The Pd(Ta)-grains have sizes up to 400 Å and the grain size increases to 600 Å after irradiation at 820 K. Above this temperature not only metastable phases are formed, but also the equilibrium PdTa phase [36], see fig. 5(c). In none of the samples could significant changes in composition due to sputtering be observed with EDX analysis (energy dispersive X-ray absorption). Oxidation is not observed after ion irradiation up to temperatures of 1020 K. Above this temperature some Ta$_2$O$_5$ [38] is observed together with the PdTa equilibrium phase. For the critical temperature for equilibrium phase formation in the Pd–Ta system we take $T_{eq} = 820$ K.

Calculations according to Miedema's model [8] show that for the alloy Pd$_{40}$Ta$_{60}$, the composition we used, the supersaturated solid solution Pd(Ta) is thermodynamically the more favorable metastable phase compared to amorphous Pd$_{40}$Ta$_{60}$. However, in this work it has been found that multilayered Pd/Ta is completely amorphized up to temperatures of 520 K. Apparently the amorphous phase forms due to the high quench rate in the ion induced collision cascade. It can be seen from the Arrhenius-curve in fig. 4, that above 520 K the temperature-dependent mixing process becomes significant. According to our model Pd-atoms will become mobile first. This gives the system enough mobility to form the more favorable metastable solid solution Pd(Ta), but not enough to form equilibrium compounds. Nucleation of Pd(Ta) seems to be enhanced by the initially crystalline nature of the sample, for it has been shown elsewhere that after ion irradiation of (co-deposited) amorphous Pd$_{40}$Ta$_{60}$ up to temperatures of 670 K no crystalline phases are detected [23]. In agree-
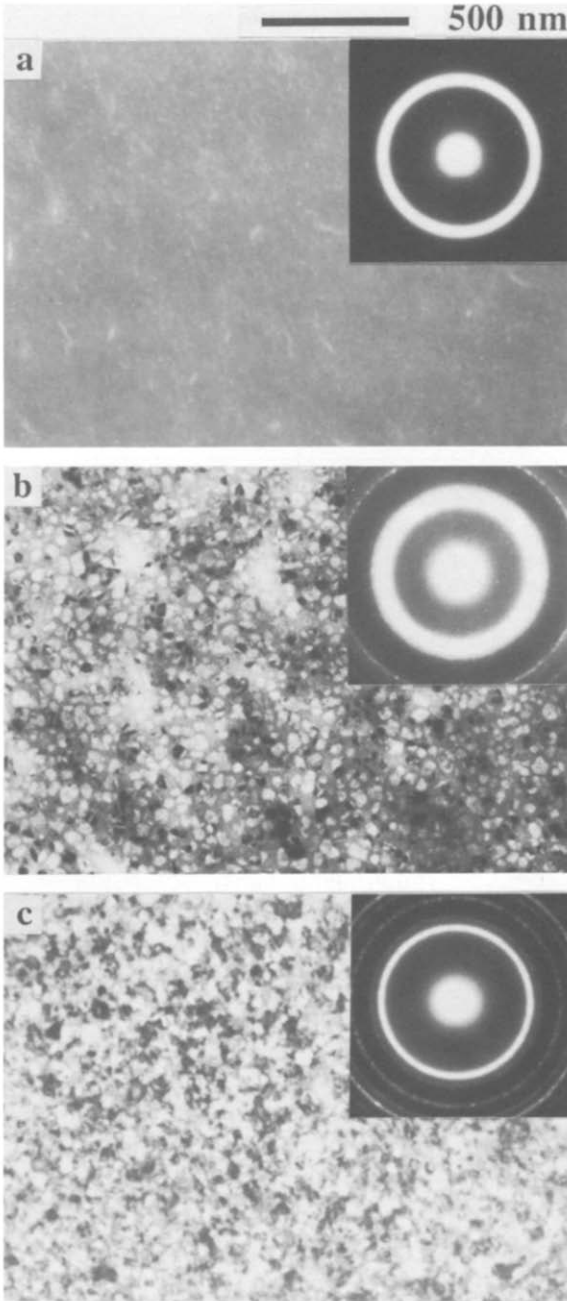
Fig. 5. TEM bright field images and diffraction patterns after ion beam mixing of Pd/Ta multilayers with 825 keV Xe$^+$ ions with doses in the order of 5×10^{15} ions/cm^2. (a) During irradiation at temperatures below 520 K the initial crystalline sample has transformed into an amorphous alloy; shown is a sample after irradiation at room temperature; (b) at 670 K amorphous Pd–Ta and a supersaturated solid solution Pd(Ta) have formed; this observation is typical for samples irradiated between 570 and 720 K; (c) at 820 K and higher the equilibrium phase PdTa is observed.

ment with the Miedema model a slight change in composition results in amorphous Pd$_{33}$Ta$_{67}$ being the more stable phase compared to a solid solution at the same composition [8]. At this composition a (diffusionless) polymorphic transition from the amorphous phase to the solid solution is not possible and the amorphous alloy has been found to be stable against ion irradiation up to 870 K [23].

4. Discussion

The experimental results of this work are summarized in table 1. Values of T_c for the Zr-alloys are taken from the literature [14–16]. The hole formation enthalpies ΔH_V for amorphous alloys $A_{1-x}B_x$ are calculated according to Miedema's model [8] using the expressions:

$$\Delta H_V^A = c_A \, \Delta H_{1V}^A + (1 - c_A)(V_A/V_B)^{5/6} \Delta H_{1V}^B \qquad (1)$$

and

$$\Delta H_V^B = c_B \, \Delta H_{1V}^B + (1 - c_B)(V_B/V_A)^{5/6} \Delta H_{1V}^A. \qquad (2)$$

ΔH_{1V}^A and ΔH_{1V}^B are the monovacancy formation enthalpies in pure A and B. The molar volume ratios (V_A/V_B) can be regarded as a measure to which degree atoms are surrounded by both constituents and the effective (surface) concentrations c_A and c_B depend on x. The accuracy of ΔH_{1V}^A and ΔH_{1V}^B is estimated to be within 5%. The data of table 1 are visualized in fig. 6, wherein T_c is plotted versus ΔH_{Vsmall} (open symbols) and T_{eq} versus ΔH_{Vlarge} (closed symbols). A linear relationship between hole formation enthalpies and the critical temperatures T_c and T_{eq} is indicated (the dashed line is drawn to guide the eye). Remarkable is the fact that where the difference in whole formation enthalpies $(\Delta H_{Vlarge} - \Delta H_{Vsmall})$ is large, the difference between T_{eq} and T_c is large. This is the case for the Zr-alloys. In the Pd–Ta system this difference is not so pronounced and T_c and T_{eq} have the same values within the error bars.

Table 1
Experimental results of this work. Critical temperatures for RED for the Zr-alloys are obtained from the literature [14–16]. Hole formation enthalpies are calculated using relations (1) and (2).

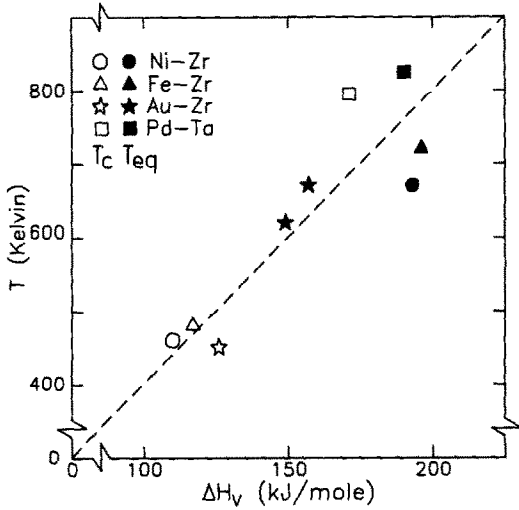| Alloy	T_c (K)	T_{eq} (k)	ΔH_{Vsmall} (kJ/mole)	ΔH_{Vlarge} (kJ/mole)
Ni$_{55}$Zr$_{45}$	460	650	110 (Ni)	193 (Zr)
Fe$_{55}$Zr$_{45}$	480	720	117 (Fe)	196 (Zr)
Au$_{50}$Zr$_{50}$	450	620	126 (Au)	149 (Zr)
Au$_{35}$Zr$_{65}$		670	134 (Au)	156 (Zr)
Pd$_{40}$Ta$_{60}$	800	820	171 (Pd)	191 (Ta)

Fig. 6. Summary of the results presented in table 1. Plotted are the critical temperatures for temperature dependent diffusion, T_c, versus formation enthalpies of holes the size of the smaller constituent, ΔH_{Vsmall} (open symbols), and the critical temperatures for equilibrium phase formation, T_{eq}, versus formation enthalpies of holes the size of the larger constituent, ΔH_{Vlarge} (closed symbols). T_{eq} values for Au–Zr represent two different compositions. The dashed line $T = 4 \times \Delta H_V$ is drawn to guide the eye.
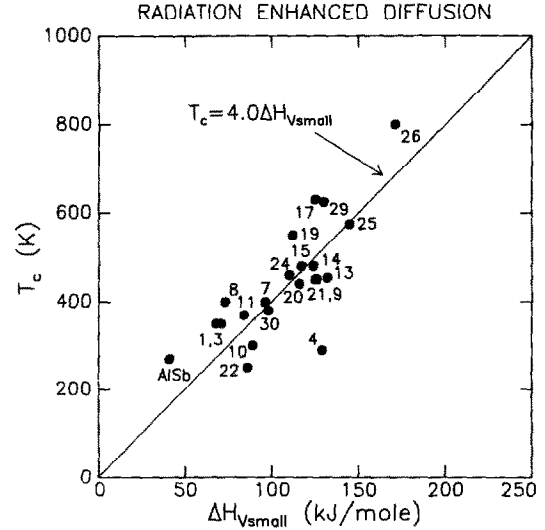

Fig. 7. Onset temperatures for radiation enhanced diffusion, T_c, versus formation enthalpy of holes the size of the smaller constituent, ΔH_{Vsmall}, for several systems reported in the literature. The maximum error in T_c is 75 K. The source of the datapoints is given by the running numbers that correspond to the first column in table 2. Also included is the non-metallic system Al–Sb (Ref. [76]; $T_c \approx 270$ K). The line $T_c = 4.0 \times \Delta H_{Vsmall}$ is a least-squares fit to the datapoints compiled in table 2.

To support our model for two critical temperatures in ion beam mixing, more data have been collected. In table 2 a compilation of data from literature on T_c and T_{eq} is given for 30 systems. For the aluminides Al–Fe, Al–V, and Al–Zr, T_{eq} is not known, but instead we have taken published temperatures at which quasicrystals form during ion beam mixing. Also in table 2 hole formation enthalpies are given. Values for ΔH were calculated by means of the expressions (1) and (2) for disordered systems at equiatomic composition. The equiatomic composition was chosen because in many of the experiments results were obtained on bilayer systems or structures consisting of single overlayers on thick substrates for which the final composition is not fixed.

In fig. 7 the values given in table 2 for T_c are plotted versus ΔH_{Vsmall}. Indeed a linear relationship is observed. The scatter in the datapoints amounts to 75 K. A least-squares fit to all datapoints yields:

$$T_c = 4.0(\pm 0.2) \times \Delta H_{Vsmall} \qquad (3)$$

in which T_c is given in kelvin and ΔH_{Vsmall} in kJ per mole.

The relationship between T_{eq}, with errors up to 50 K, and ΔH_{Vlarge} can be seen in fig. 8,

$$T_{eq} = 3.8(\pm 0.2) \times \Delta H_{Vlarge} \qquad (4)$$

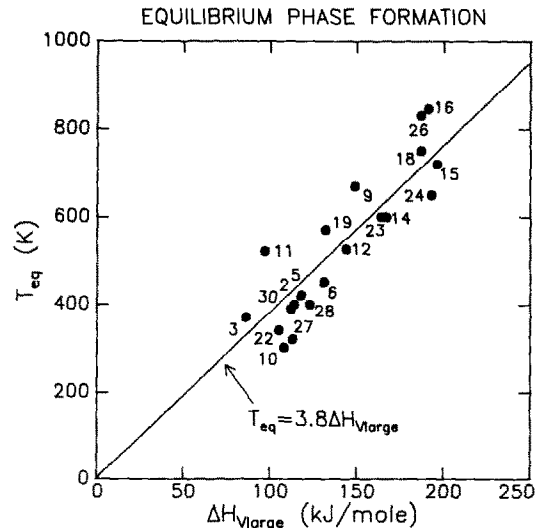is found. Using the relationships (3) and (4) in combina-

Fig. 8. Critical temperatures, T_{eq}, above which equilibrium phases will be formed during ion beam mixing versus formation enthalpy of holes the size of the larger constituent, ΔH_{Vlarge}, for several systems reported in literature. The maximum error in T_{eq} is 50 K. The source of the datapoints is given by the running numbers that correspond to the first column in table 2. The line $T_{eq} = 3.8 \times \Delta H_{Vlarge}$ is a least-squares fit to the datapoints.

Table 2
Literature overview of critical temperatures for radiation enhanced diffusion (T_c) and metastable alloy formation (T_{eq}). Hole formation enthalpies are calculated at equiatomic composition for random alloys according to the Miedema model [8] using relations (1) and (2). All systems have negative or near zero heat of mixing. The numbering of the alloys corresponds with the numbering of the datapoints in fig. 7 and 8.

Alloy		T_c (K)	Refs.	T_{eq} (K)	Refs.	ΔH_{Vsmall} (kJ/mole)	ΔH_{Vlarge} (kJ/mole)
1	Al–Cu	350	[45]	–	–	71 (Cu)	93 (Al)
2	Al–Fe	–	–	400	[46,47]	89 (Fe)	114 (Al)
3	Al–Mn	350	[48]	370	[48,49,50,51]	68 (Mn)	86 (Al)
4	Al-Mo	290	[52]	–	–	129 (Mo)	132 (Al)
5	Al–V	–	–	420	[53]	102 (V)	118 (Al)
6	Al–Zr	–	–	450	[47,54]	103 (Al)	131 (Zr)
7	Au–Ni	400	[55]	–	–	96 (Ni)	137 (Au)
8	Au–Si	400	[56,57]	–	–	73 (Si)	86 (Au)
9	Au–Zr	450	[16]	620	this work	126 (Au)	149 (Zr)
10	Co–Si	300	[58]	300	[58]	89 (Co)	108 (Si)
11	Cr–Si	370	[59]	520	[59]	84 (Cr)	97 (Si)
12	Cu–Ti	–	–	525	[60,61,62]	107 (Cu)	144 (Ti)
13	Fe–Pt	454	[63]	–	–	132 (Fe)	168 (Pt)
14	Fe–Ti	480	[64]	600	[64]	124 (Fe)	167 (Ti)
15	Fe–Zr	480	[15]	720	this work	117 (Fe)	196 (Zr)
16	Mo–Ni	–	–	830	[65]	143 (Ni)	187 (Mo)
17	Mo–Si	630	[66,67]	–	–	125 (Si)	134 (Mo)
18	Nb–Ni	–	–	750	[18]	129 (Ni)	187 (Nb)
19	Nb–Si	550	[1]	570	[1]	112 (Si)	132 (Nb)
20	Ni–Pd	440	[63,68]	–	–	116 (Ni)	150 (Pd)
21	Ni–Pt	450	[55]	–	–	125 (Ni)	166 (Pt)
22	Ni–Si	250	[69]	340	[59,70,71]	86 (Ni)	105 (Si)
23	Ni–Ti	–	–	600	[18,65]	117 (Ni)	164 (Ti)
24	Ni–Zr	460	[14]	650	this work	110 (Ni)	193 (Zr)
25	Pd–Pt	575	[10]	–	–	145 (Pd)	149 (Pt)
26	Pd–Ta	800	this work	820	this work, [23]	171 (Pd)	191 (Ta)
27	Pt–Si	–	–	320	[59,71]	104 (Si)	113 (Pt)
28	Ru–Si	–	–	400	[72]	121 (Ru)	123 (Si)
29	Si–Ta	625	[11]	–	–	130 (Si)	154 (Ta)
30	Si–Ti	380	[73,74,75]	390	[74]	98 (Si)	112 (Ti)

tion with the expressions (1) and (2) to calculate the hole formation enthalpies, it is possible to predict temperature ranges in which fast mixing occurs via RED, and yet metastable alloys are formed.

Our results show the existence of two critical temperatures in ion beam mixing. Both temperatures are correlated with hole formation enthalpies. This may be understood as follows. The interdiffusion coefficient for RED is given by the relation:

$$\tilde{D} \propto (X_B D_A + X_A D_B).$$

X_A and X_B are the mole fractions of element A and B. D_A and D_B are the self-diffusion coefficients for RED, which can be written in the form:

$$D_i = D_{i,0} \exp(-Q_i/kT). \tag{5}$$

The corresponding activation energies Q_A and Q_B are given by ΔH_{MA} and ΔH_{MB}, the migration enthalpies for A and B atoms respectively. Because not much is known about migration enthalpies in amorphous alloys, we approximate ΔH_{MA} and ΔH_{MB} by the hole formation enthalpies ΔH_{VA} and ΔH_{VB}, which are calculated using the expressions (1) and (2). The replacement of migration enthalpies by hole formation enthalpies is based on the following. In an excellent review by Brown and Ashby [39] it has been shown clearly that the ratio Q_{SD}/RT_m (Q_{SD} is the activation energy for substitutional diffusion and T_m is the melting point) is constant over a wide range of systems. Together with the well-known observation that ΔH_V scales with T_m [40], it can be easily derived that ΔH_V is proportional to ΔH_M. If

both Q_{SD}, which is $\Delta H_V + \Delta H_M$, and ΔH_V are proportional to T_m, ΔH_M must be proportional to ΔH_V. Moreover, observations by Shewmon [41] and more recently by Franklin [42], showed for several metals that ΔH_M and ΔH_V are equal within 10% accuracy.

The linear relationships (3) and (4) indicate that in ion beam mixing the apparent activation energies of the temperature-dependent diffusion processes are the determining factors for the related critical temperatures. The preexponential factors for the self-diffusion coefficients, which will depend on the system studied and the particular experimental conditions, seem to be of less importance. This has also been shown by Rauschenbach [43], who found a dependence of T_c on ΔH_V^m, the average migration enthalpy of vacancies. So, assuming a constant $D_{i,0}$ for each system, and equal for atoms A and B, D_i will depend critically on the ratio $(\Delta H_V/kT)$, resulting in the linear relationships (3) and (4) between temperature and hole formation enthalpy.

The predictions for T_c and T_{eq} should not be regarded as absolute values but rather as estimates, as can be seen by the deviations from the model up to 100 K in figs. 7 and 8. Furthermore, important parameters, such as the nucleation and growth mechanisms are ignored in the present model. Note that in some cases above T_c a metastable crystalline phase nucleates first. Then there must be still a higher temperature at which equilibrium is truly achieved. Detailed information about the processes involved can only be obtained by studying individual systems. For example, the complexity of ion induced diffusion processes in elementary Ni is demonstrated by Müller et al. [44]. Nonetheless, from their data a T_c of 600 K can be inferred, a value which is still within the predicted range of 525($\pm$75) K of our model.

Although different criteria are applied to determine T_c and T_{eq}, it is possible to compare the proportionality constants $C_c = 4.0(\pm 0.2)$ and $C_{eq} = 3.8(\pm 0.2)$ from relations (3) and (4). Because the measured effects (diffusion cq. crystallization) are on comparable length and time scales (in the order of 100 Å and 1 h respectively) we expect C_c and C_{eq} to be approximately the same. Within the error bars this is indeed the case. It should be mentioned that for individual systems the preexponential factors for the self-diffusion coefficients (5) will depend on experimental conditions and a dose rate dependence might be expected for both T_c and T_{eq}.

Previous investigations have shown that for the crystallization temperature, T_x, for amorphous alloys via a diffusion controlled process the following relationship holds [17,77]:

$$T_x \approx 4.7 \times \Delta H_{Vlarge}. \tag{6}$$

In the model that is put forward in these papers crystallization is governed by diffusivity of the larger constituent. The self-diffusion coefficient for this constituent will have the same form as (5) and the corresponding activation energy will be Q_x. Because for the determination of T_x and T_{eq} the same effect is investigated (growth of crystals larger than 100 Å on time scales of typically 1 h) a direct comparison can be made of the activation energies for thermal and ion induced crystallization of amorphous alloys under the assumption that the pre-exponential factors for both diffusion processes are approximately equal. As argued before, a linear relationship between crystallization temperature and hole formation enthalpy indicates that the activation energy is most important. It then can be derived that the ratio of the activation energies equals the ratio of the proportionality constants from eqs. (4) and (6):

$$Q_x/Q_{eq} \approx C_x/C_{eq} \approx 1.2,$$

wherein the activation energy for the ion-induced crystallization process is labeled Q_{eq}. The relative difference between Q_x and Q_{eq} is unexpectedly small and might be influenced by the inaccuracy of the proportionality constants C_x and C_{eq}. A larger difference is expected when the activation energy of the ion induced process is considered as a migration enthalpy only, and the activation energy of the thermal process as the same migration enthalpy plus an additional energy associated with the creation of holes or vacancies required for vacancy-like diffusion in amorphous alloys. This clearly requires further investigation.

5. Conclusions

Ion mixing with high energy heavy ions has been shown to lower the crystallization temperature of the amorphous alloys Ni–Zr, Fe–Zr, Au–Zr, and Pd–Ta significantly. Furthermore, it has been shown that in ion beam mixing of binary systems two critical temperatures can be defined. These temperatures can be predicted by the expressions:

$$T_c \approx 4.0 \times \Delta H_{Vsmall}$$

and

$$T_{eq} \approx 3.8 \times \Delta H_{Vlarge},$$

in which the temperatures are given in kelvin and the hole formation enthalpies in kJ/mole. At T_c the smaller constituent becomes mobile and RED sets in. However, metastable phases will form and remain stable under influence of the ion beam below T_{eq}. Above this temperature also the larger constituent can migrate over large distances and equilibrium phases will form. For systems with a large difference between hole formation enthalpies $\Delta H_{Vlarge} - \Delta H_{Vsmall}$ metastable alloys can be formed rather efficiently using RED. The values for T_c and T_{eq} as predicted with our model should not be regarded as absolute values but rather as guidelines to

select systems in which phenomena as RED and metastable alloy formation occur simultaneously.

Acknowledgments

References

[1] S. Matteson, J. Roth, and M.-A. Nicolet, Radiat. Eff. 42 (1979) 217.

[2] R.S. Averback, Nucl. Instr. and Meth. B15 (1986) 675.

[3] Surface Alloying by Ion, Electron, and Laser Beams, eds. L.E. Rehn, S.T. Picraux, and H. Wiedersich, (American Society for Metals, Metals Park, Ohio 1987).

[4] M. van Rossum and Y.-T. Cheng, Defect and Diffusion Forum 57–58 (1988) 1.

[5] L.E. Rehn and P.R. Okamoto, Nucl. Instr. and Meth. B39 (1989) 104.

[6] W.L. Johnson, Y.-T. Cheng, M. van Rossum, and M-A. Nicolet, Nucl. Instr. and Meth. B7/8 (1985) 657.

[7] B.M. Paine and B.X. Liu, in Ion Beam Assisted Film Growth, ed. T. Itoh (Elsevier, Amsterdam, 1989) p. 153.

[8] F.R. de Boer, R. Boom, W.C.M. Mattens, A.R. Miedema, and A.K. Niessen, Cohesion in Metals, eds. F.R. de Boer and D. Pettifor (North-Holland, Amsterdam, 1988).

[9] P.I. Loeff, A.W. Weeber, and A.R. Miedema, J. Less-Common Met. 140 (1988) 299.

[10] Y.-T. Cheng, X.-A. Zhao, T. Banwell, T.W. Workman, M-A. Nicolet, and W.L. Johnson, J. Appl. Phys. 60 (1986) 2615.

[11] Y.-T. Cheng, Phys. Rev. B40 (1989) 7403.

[12] M. Doyama and J.S. Koehler, Acta Metall. 24 (1976) 871.

[13] R.S. Averback and H. Hahn, Phys. Rev. B37 (1988) 10383.

[14] F.-R. Ding, R.S. Averback, and H. Hahn, J. Appl. Phys. 64 (1988) 1785.

[15] F.-R. Ding, P.R. Okamoto, and L.E. Rehn, Nucl. Instr. and Meth. B39 (1989) 122.

[16] F.-R. Ding, P.R. Okamoto, and L.E. Rehn, Mater. Res. Soc. Symp. Proc. 100 (1988) 69.

[17] R.B. Schwarz and W.L. Johnson, Phys. Rev. Lett. 51 (1983) 415;
J.C. Barbour, R. de Reus, A.W. Denier van der Gon, and F.W. Saris, J. Mater. Res. 2 (1987) 168;
O. Thomas, F.M. d'Heurle and A. Charai, Philos. Mag. B58 (1988) 529.

[18] J. Bøttiger, K. Dyrbye, K. Pampus, and R. Poulsen, Philos. Mag. A59 (1989) 569.

[19] K.H.J. Buschow, J. Phys. F. Met. Phys. 14 (1984) 593.

[20] Z. Altounian, Tu Guo-Hua, and J.O. Strom-Olsen, J. Appl. Phys. 54 (1983) 3111.

[21] K.H.J. Buschow, J. Less-Common Met. 79 (1981) 243.

[22] E. Hellstern and L. Schultz, Appl. Phys. Lett. 49 (1986) 1163.

[23] J.P.W.B. Duchateau, H.C. Tissink, G.J. van der Kolk, J. Verhoeven and F.W. Saris, Proc. 7th Int. Conf. on Ion and Plasma Assisted Techniques (CEP Consultants Ltd., Edinburgh, UK, 1989) p. 373.

[24] A. Polman, A.M. Vredenberg, W.H. Urbanus, P.J. van Deenen, S. Doorn, J. Derks, J. ter Beek, H. Alberda, H. Krop, I. Attema, E. de Haas, H. Kersten, S. Roorda, R. Schreutelkamp, J.G. Bannenberg, and F.W. Saris, Nucl. Instr. and Meth. B37/38 (1989) 935.

[25] J.F. Ziegler, J.P. Biersack, and U. Littmark, The Stopping and Range of Ions in Solids, vol. 1 (Pergamon Press, New York, 1985).

[26] L.R. Doolittle, Nucl. Instr. and Meth. B9 (1985) 344.

[27] Powder diffraction file 27-997, (International Centre for Diffraction Data, Swarthmore, USA).

[28] Diffraction patterns for Ni_2Zr, Ni_5Zr, and $Ni_{10}Zr_7$ (spacegroup Pbca) calculated after crystallographic data from Pearson's Handbook of Crystallographic Data for Intermetallic phases by P. Villars and L.D. Calvert (American Society for Metals, Metals Park, 1985).

[29] Z. Altounian, E. Batalla, J.O. Strom Olsen, and J.L. Walter, J. Appl. Phys. 61 (1987) 149.

[30] J. Bøttiger, N.J. Mikkelsen, S.K. Nielsen, G. Weyer, and K. Pampus, J. Non-Cryst. Solids 76 (1985) 303.

[31] B. Walz, P. Oelhafen, H.-J. Güntherodt, and A. Baiker, Appl. Surf. Sci. 37 (1989) 337.

[32] R. de Reus, H.C. Tissink, and F.W. Saris, J. Mater. Res. 5 (1990) 341.

[33] Powder diffraction file 26-809.

[34] Powder diffraction file 28-442.

[35] Powder diffraction file 5-681.

[36] Powder diffraction file 4-788.

[37] Powder diffraction file 16-868.

[38] Powder diffraction file 25-922.

[39] A.M. Brown and M.F. Ashby, Acta Metall. 28 (1980) 1085.

[40] C.P. Flynn, Point Defects and Diffusion (Clarendon Press, Oxford, 1972) p. 78.

[41] P.G. Shewmon, Diffusion in Solids (McGraw Hill, New York, 1963) p. 74.

[42] A.D. Franklin, in: Point Defects in Solids, Vol. 1. General and Ionic Crystals, eds. J.H. Crawford, Jr. and L.M. Slifkin (Plenum Press, New York–London, 1972), p. 27.

[43] B. Rauschenbach, Phys. Status Solidi 102 (1987) 645.

[44] A. Müller, V. Naundorf, and M.-P. Macht, J. Appl. Phys. 64 (1988) 3445.

[45] F. Besenbacher, J. Bøttiger, S.K. Nielsen, and H.J. Whitlow, Appl. Phys. A29 (1982) 141.

[46] K. Hohmuth, V. Heera, and B. Rauschenbach, Nucl. Instr. and Meth. B39 (1989) 136.

[47] D.A. Lilienfield, L.S. Hung, and J.W. Mayer, Nucl. Instr. and Meth. B19/20 (1987) 1.

[48] Y. Kido, Nucl. Instr. and Meth. B37/38 (1989) 696.

[49] D.M. Follstaedt and J.A. Knapp, J. Appl. Phys. 59 (1986) 1756.

[50] D.A. Lilienfield, M. Nastasi, H.H. Johnson, D.G. Ast, and J.W. Mayer, Phys. Rev. Lett. 55 (1985) 1587.

[51] J.D. Budai and M.D. Aziz, Phys. Rev. B33 (1986) 2877.

[52] E. Ma, A.J. Brunner, T.W. Workman, C.W. Nieh, X.-A. Zhao, and M-A. Nicolet, Mater. Res. Soc. Symp. Proc. 100 (1988) 75.

[53] N. Karpe, L.-U. Aaen Andersen, K. Dyrbye, J. Bøttiger, and K.V. Rao, Phys. Rev. B39 (1989) 9874.

[54] D.A. Lilienfield and J.W. Mayer, Mater. Res. Soc. Symp. Proc. 74 (1987) 339.

[55] J. Bøttiger, S.K. Nielsen, and P.T. Thorsen, in: Amorphous Materials and Non-Equilibrium Processing, edited by M. von Allmen, (Les Editions de Physique, Les Ulis Cedex, 1984) p. 111.

[56] F. Priolo, J.M. Poate, D.C. Jacobson, J. Linnros, J.L. Batstone, and U. Campisano, Mater. Res. Symp. Proc. 100 (1988) 87.

[57] A.J. Barcz, B.M. Paine, and M-A. Nicolet, Appl. Phys. Lett. 44 (1985) 45.

[58] A.H. Hamdi and M-A. Nicolet, Thin Solid Films 119 (1984) 357.

[59] J.W. Mayer, B.Y. Tsaur, S.S. Lau, and L-S. Hung, Nucl. Instr. and Meth. 182/183 (1981) 1.

[60] J. Koike, P.R. Okamoto, and M. Meshii, Mater. Res. Soc. Symp. Proc. 100 (1988) 57.

[61] J. Koike, P.R. Okamoto, L.E. Rehn, and M. Meshii, Mater. Res. Soc. Symp. Proc. 128 (1989) 339.

[62] J. Koike, P.R. Okamoto, L.E. Rehn, and M. Meshii, J. Mater. Res. 4 (1989) 1143.

[63] A.M. Ibrahim, Nucl. Instr. and Meth. B34 (1988) 135.

[64] U. Scheuer, L.E. Rehn, and P. Baldo, Mater. Res. Soc. Symp. Proc. 128 (1989) 213.

[65] J.L. Brimhall, Nucl. Instr. and Meth. B7/8 (1985) 26.

[66] G. Vályi, H. Ryssel, and W. Möller, Nucl. Instr. and Meth. B39 (1989) 268.

[67] B.V. King, D.G. Tonn, and I.S.T. Tsong, Nucl. Instr. and Meth. B7/8 (1985) 607.

[68] U.G. Akano, D.A. Thompson, W.W. Schmeltzer, and J.A. Davies, J. Mater. Res. 3 (1988) 1063.

[69] R.S. Averback, L.J. Thompson, Jr., J. Moyle, and M. Schalit, J. Appl. Phys. 53 (1982) 1342.

[70] L.S. Hung, J.W. Mayer, C.S. Pai, and S.S. Lau, J. Appl. Phys. 58 (1985) 1527.

[71] K. Affolter, X-A. Zhao, and M-A. Nicolet, J. Appl. Phys. 58 (1985) 3087.

[72] M. Nastasi, D.A. Lilienfield, H.H. Johnson, and J.W. Mayer, J. Appl. Phys. 59 (1986) 4011.

[73] K. Maex, R.F. de Keersmaeker, M. van Rossum, and W.F. van der Weg, Mater. Res. Soc. Symp. Proc. 100 (1988) 63.

[74] K. Kohlhof, S. Mantl, and B. Stritzker, Mater. Res. Soc. Symp. Proc. 74 (1987) 443.

[75] K. Maex, R.F. de Keersmaeker, M. van Rossum, W.F. van der Weg, and G. Krooshof, Nucl. Instr. and Meth. B19/20 (1987) 731.

[76] B.M. Paine, M-A. Nicolet, and T.C. Banwell, Mater. Res. Soc. Symp. Proc. 7 (1982) 79.

[77] R. de Reus and F.W. Saris, Mater. Lett. 9 (1990) 487.